JOINT EUROPEAN TORUS

JET–P(89)35

G.A. Cottrell, V.P. Bhatnagar, M. Bures, L.G. Eriksson, T. Hellsten,
J. Jacquinot D.F.H. Start and JET Team

Non-Thermal DT Yield with (D)T ICRH Heating in JET

Non-Thermal DT Yield with (D)T ICRH Heating in JET

G.A. Cottrell, V.P. Bhatnagar, M. Bures, L.G. Eriksson, T. Hellsten, J. Jacquinot, D.F.H. Start and JET Team*

JET-Joint Undertaking, Culham Science Centre, OX14 3DB, Abingdon, UK

** See Appendix 1*

Preprint of Paper to be submitted for publication in
Plasma Physics and Controlled Fusion

NON–THERMAL DT YIELD WITH (D)T ICRH HEATING IN JET

G.A.Cottrell, V.P.Bhatnagar, M.Bures, L.G.Eriksson[+], T.Hellsten,
J.Jacquinot and D.F.H.Start.

JET Joint Undertaking, Abingdon, Oxon., OX14 3EA, United Kingdom.
[+]Chalmers University, Sweden.

Abstract – Projections of the (D)T fusion yield expected during fundamental ICRH heating of D in JET tritium plasmas are presented. The highest fusion multiplication factor, Q ($\equiv P_{fus} / P_{rf}$), is achieved for a relatively high plasma density ($n_{e_0} > 5\times10^{19}$ m^{-3}) and minority concentration ratio $n_D/n_T \cong 20\%$ –40% with dipole antenna ($k_{\|} \approx 7m^{-1}$). The latter reduces mode conversion and maximises the rf power coupled to the minority ions. We have used ray–tracing and global wave ICRH codes to calculate power deposition profiles; 80% is cyclotron damped by deuterium and 17% is coupled directly to electrons via TTMP and Landau damping. With launched rf power P_{rf}=12MW deposited ≈0.3m off–axis, we predict fusion powers P_{fus} up to ≈ 8MW for a range of JET plasmas with achieved plasma pressure $n_{e_0}T_{e_0} = 6\times10^{20}$keV m^{-3} and Z_{eff}=2. Projecting to P_{rf} = 25MW, P_{fus} increases to 17MW with Z_{eff}=2.

1. INTRODUCTION

In a two–ion component plasma, the fast magnetosonic wave can be damped on a minority ion species at its fundamental cyclotron resonance causing the minority ion distribution function to develop a non–Maxwellian velocity distribution with a high energy tail. The tail will also enhance the fusion reaction rate with the background ion species (STIX, 1975). Earlier JET experiments (COTTRELL *et al.*, 1988) using ICRH heating in the $(^3He)D$ minority regime have produced $\cong$ 1MJ of fast ^3He ions in the plasma (with particle energies up to a few MeV) and a ^3He–D reaction rate $R < 2\times10^{16}$ s^{-1} ($\approx$ 60kW of fusion power). Measured fast ion energy content and fusion reactivity in these experiments have since been modelled in detail (BOYD *et al.*, 1989; ERIKSSON *et al.*, 1989) using Fokker–Planck and global wave codes. Good agreement between experiment and theory was found, consistent with i) classical slowing down of fast ions and ii) the cyclotron damping profiles on the ^3He. The possibility of producing enhanced fusion reactivity using the deuterium cyclotron resonance (D)T scheme has been suggested (JET TEAM, 1988) for the JET active phase but the method is also of potential importance in reactor ignition studies. This paper discusses optimisation of the scheme with particular reference to JET.

2. UNDERLYING THEORY

Cyclotron damping of the incident magnetosonic wave can transfer energy to the resonant minority ion distribution. The ions essentially increase their velocities perpendicular to the direction of the tokamak magnetic field. This group of minority ions becomes much hotter than the bulk plasma electrons ($E > kT_e$) and the distribution becomes non–Maxwellian. A description of the development of an energetic distribution of this type has been described earlier (STIX, 1975) where the Fokker–Planck terms of the Boltzmann equation included a quasi–linear rf diffusion coefficient to describe the diffusion of ions in velocity phase space as they cross the rf resonance layer. In the limit of high energy, the rf power is not isotropized. The minority (tail) distribution can still be approximated by a bi–Maxwellian function. The effective perpendicular temperature of the tail is then determined by the electron density, temperature and RF power. At lower energies, the minority distribution becomes isotropized by collisional pitch angle scattering and the slope of the distribution function then becomes sensitive to the composition of the background ions.

In the velocity range of interest for $(D)T$ non–thermal processes: $v_{Ti} < v << v_{Te}$, where v_{Ti} and v_{Te} are, respectively, the bulk ion and electron thermal velocities, the following expression relates the local minority tail temperature,

$$T_t = T_e \frac{1 + (v_\beta / v)^3 + \epsilon \xi_{rf}}{1 + (v_\alpha / v)^3}, \tag{1}$$

to the Stix parameter,

$$\xi_{rf} = \rho_{rf} \tau_s / 3\, n_m (kT_e), \tag{2}$$

where ρ_{rf} is the local value of the rf power density coupled to the minority ions, τ_s the classical ion–electron slowing–down time and n_m the number density of minority ions. The parameter ϵ is related to the number of degrees of freedom available to the fast ions and depends on assumptions about the degree of isotropy of the tail; at very high energies ($\xi_{rf} >> 1$) $\epsilon = 3/2$, and at lower energies $\epsilon = 1$. The characteristic velocities v_α and v_β in Eq.(1) are defined (ANDERSON 1983) by

$$v_\alpha^3 = \frac{3\sqrt{\pi}}{4} \left[\frac{2kT_e}{m_e} \right]^{3/2} \sum_j \frac{n_j}{n_e} Z_j^2 \frac{m_e}{m_j} \tag{3}$$

$$v_\beta^3 = \frac{3\sqrt{\pi}}{4} \left[\frac{2kT_e}{m_e} \right]^{1/2} \sum_j \frac{n_j}{n_e} Z_j^2 \frac{2kT_j}{m_j} \tag{4}$$

where Z_j is the atomic charge of background ions of mass m_j having number density n_j and temperature T_j. When $T_i = T_e$, $v_\alpha = v_\beta = v_c$. The critical velocity, v_c, is related to the critical energy by $E_c = mv_c^2/2$ where

$$E_c = 14.8\, T_e \left[(A_f^{3/2} / n_e) \sum_j (n_j Z_j^2 / A_j) \right]^{2/3} \tag{5}$$

and A_f and A_j are the atomic mass numbers of the fast and background ion species respectively. Eqs. (1) to (5) show the role of the background ions on the friction experienced by the fast ions. When $E >> E_c$, the slowing–down rate is determined by ion–electron friction; conversely when $E << E_c$, the slowing–down rate is dominated by ion–ion collisions. In the case $\xi_{rf} = 0$ and with common ion and electron temperatures, Eq.(1) shows that the minority tail relaxes back to the bulk

electron temperature, $T_t = T_e$.

To illustrate the expected reactivity of the non–thermal tail from Stix's theory, we initially approximate it by a Maxwellian. The number of fusion reactions per unit volume per second is given by

$$R_{DT} = n_D\, n_T < \sigma v >, \tag{6}$$

where n_D and n_T are the number densities of deuterium (in this case the minority species i.e. $n_D = n_m$) and tritium (the majority species) respectively and $< \sigma v >$ is the fusion cross–section–velocity product averaged over two Maxwellian distributions of temperature T_t (for the deuterium tail) and T_i for the warm background majority ions. When $\epsilon\, \xi_{rf} >> 1$, Eqs. (1)–(6) give

$$R_{DT} = \epsilon C\, (n_T / n_e)\, \rho_{rf}\, T_e^{3/2}\, s\,(T_t) \tag{7}$$

where we have incorporated in the function s all the cross–section and energy–dependent terms,

$$s\,(T_t) = \frac{< \sigma v >}{T_t[1 \;+\; (E_\alpha / T_t)^{3/2}] \;-\; T_e[1 \;+\; (E_\beta / T_t)^{3/2}]}, \tag{8}$$

the constant $C = 3.16 \times 10^{14}\, (A_f / Z_f^2 \ell n\, \Lambda\,)$ and $\ell n\, \Lambda$ is the Coulomb logarithm.

Fig.1 shows the function $s\,(T_t)$, computed using a modified version of the fusion cross–section (ASHER–PERES, 1979; SADLER 1989) assuming $T_i = T_e$ and $Z_{eff} = 2$ for a plasma composed of D,T and impurity C species. For background ion temperatures in the range 5 keV – 10 keV, s has a maximum which occurs for an optimum tail temperature $T_t \cong 100$ keV. For fixed plasma conditions, R_{DT} has a maximum which we associate with an optimum tail temperature. At this optimum, R_{DT} may only be significantly increased by maximising the tritium concentration term (n_T / n_e); this underlines the importance of producing clean plasmas with low impurity content. The increase in reactivity with electron temperature also implied in Eq.(7) is, however, likely to be limited because the electron temperature in typical JET discharges is beyond the level where ion–ion collisions start to dominate the slowing–down of minority particles having energies near the maximum in the fusion cross–section, i.e. $T_t \cong E_c$. This is evident for the two cases in Fig.1: increasing the

common temperature from 5 keV to 10 keV increases $T_e^{3/2}$ in Eq.(7) by a factor 2.8 whilst the maximum value of the function s decreases by a factor 1.8. The net gain in reactivity is therefore only a factor of 1.6.

Using the curves of Fig.1 and Eq.(7), we next estimate a value for the maximum theoretical Q_{rf}. For typical JET central conditions: $T_e = T_i = 10$ keV; $Z_{eff} = 2$ and $\ell n\, \Lambda = 16$, but with a hypothetical DT composition: $n_D = 1.8 \times 10^{19}$ m^{-3}; $n_T = 3 \times 10^{19}$ m^{-3}; $n_C = 0.2 \times 10^{19}$ m^{-3}; $n_T / n_e = 0.5$, the maximum value in the energy and cross–section term, $s\,(T_t)|^{\max} = 3 \times 10^{-24}$ m^{3}s^{-1}keV^{-1}, occurs at a tail temperature of $T_t \cong 100$ keV where the maximum fusion multiplication factor is

$$Q_{rf}|^{\max} = \epsilon C\,(n_T / n_e)\; Y\, T_e^{3/2}\, s\,(T_t)|^{\max} \qquad (9)$$

where the fusion energy liberated is $Y = 17.6$ MeV per reaction. For the plasma parameters described above, we find $E_c = 165$ keV and $Q_{rf}|^{\max} = 1.1$. For a similar plasma but having lower temperatures $T_e = T_i = 5$keV we obtain $E_c = 83$ keV and $Q_{rf}|^{\max} = 0.6$.

Naturally this simple estimate of $Q_{rf}|^{\max}$ is only relevant in an ideal homogeneous plasma slab. The local description remains useful because it provides a reference value for $Q_{rf}|^{\max}$ which can be compared with results of other models. For realistic tokamak plasmas having radial profiles of temperature, density and rf power density, the optimum conditions implied by Eq.(9) are unlikely to be obtained in the whole volume where rf is absorbed on the deuterium. Thus, in general, the value of $Q_{rf}|^{\max}$ represents an upper bound on the experimentally attainable Q. We next discuss a more realistic model of the tokamak plasma, which includes aspects of wave damping and the effects of experimental plasma and rf deposition profiles.

3. MODELLING

3.1 *Wave Damping*

The discussion of section 2 highlights the important requirement that, in order to maximise Q for DT reactions, it is essential to create an optimal minority distribution having temperatures typically $\cong$ 100 keV. For typical JET plasma conditions and rf power densities, this requirement makes it necessary to consider using

higher ($n_D/n_e \approx$ 10%–30%) minority concentrations than have been used in previous JET experiments. In the absence of experimental data in these conditions, we have therefore estimated wave damping in simulated (D)T plasmas using both global wave and ray–tracing codes. We assume that it will be possible to produce *DT* plasmas having the same confinement properties (i.e. the same densities and temperatures for the same fixed input power) as those which have already been obtained using deuterium in JET. We have therefore based our modelling on a reference set of parameters (discharge A; Table I) which, apart from the different ionic species, closely resembles the current–rise (type II) discharge described in section 4.

TABLE I

Plasma parameters for reference discharge A

Coupled RF power, *Prf*	12MW
Damped RF power on *D* minority, P_D	10MW
Central electron density, n_{e_0}	6×10^{19} m^{-3}
Central electron Temperature, T_{e_0}	10 keV
Central ion Temperature, T_{i_0}	10 keV
Temperature profile exponent, γ_T	2.0
Density profile exponent, γ_n	4.0
Deuterium–to–Tritium density ratio, η	0.23

Initially, we have calculated single–pass damping rates for a fixed value of $k_\parallel$ = 7m^{-1} (corresponding to the maximum in the radiated spectrum of the JET dipole antenna) using the 1D FREMIR code which is based on the theoretical model of JACQUINOT (1978). The code uses the WKB approximation to calculate the rf power damped on the *D* minority ions through cyclotron absorption and electron Landau damping and TTMP to calculate the rf power damped on the electrons.

The cyclotron resonance, $\omega = \omega_{cD}$, was placed at the plasma centre R = 3m corresponding to a central magnetic field $B_\varphi(0)$ = 3.3 Tesla and RF frequency f = 25 MHz, parameters which are relevant to the JET system. Fig.2 shows the normalised absorbed power plotted as a function of radius from the launch point of the wave on

the low field side of the torus ($R = 4.1$m). The single–pass absorption on the deuterium was $P_D/P_{rf} = 87\%$ for $k_{||} = 7$ m^{-1}. The electrons absorbed $P_e/P_{rf} = 6\%$ whilst 7% remained unabsorbed after a single pass of the wave. The sensitivity of the single–pass absorption to $k_{||}$ variations is shown in Fig.3. The deuterium damping is significant over a wide range of $k_{||}$ exhibiting a broad maximum centered on $k_{||} \cong 5$ m^{-1} and reaching a maximum value of $P_D/P_{rf} = 88\%$. Below $k_{||} \cong 2$ m^{-1}, P_D/P_{rf} falls below 80%. In the range $k_{||} \cong 1$ m^{-1}–8 m^{-1}, the electron damping is below 10%. At a fixed value of $k_{||} = 7$ m^{-1}, we also investigated the sensitivity of the damping on the ion mixture ratio, $\eta = n_D/n_T$, in the range 0.05–0.4 (Fig.4). Above $\eta = 0.15$, $P_D/P_{rf} > 80\%$ whilst P_e/P_{rf} is below 10%.

The result of a ray–tracing calculation (BHATNAGAR *et al.*, 1984) of the full $k_{||}$ spectrum of the JET toroidal dipole antenna is shown in Fig.5. Of the launched rf power, 80% was damped in a single pass on the D minority, 17% was deposited on the electrons via TTMP and Landau damping and 3% was unabsorbed. Accordingly, in the cases studied below, we define the rf power fraction damped on the deuterium minority ions as $P_D/P_{rf} = 0.8$.

3.2 *The Stix Model*

Because the DT reaction rate is sensitive to the profiles of electron and ion temperature and density, and the rf deposition, the effects of both rf and tokamak profiles must be taken into account in any realistic model. In the model described here, this was done by calculating the fusion reaction rate in a large number of circular radial shells centered on the magnetic axis of the plasma. The circular approximation is reasonable in the central zone of the plasma ($x = r/a < 0.5$) where flux surface geometry has small elongation and triangularity ratios and the highest rf and DT fusion power densities will be produced. The plasma profiles for ions and electrons were modelled with the common parabolic form

$$y(x) = y(a) + [y(0) - y(a)].(1 - x^2)^{\gamma} \qquad (10)$$

where $y(a)$ and $y(0)$ represent edge and central values respectively. The exponent γ was determined by fitting to experimental data. The plasma model contained an admixture of three ionic species: D, T and C impurity. Given a fixed and required ratio of n_D/n_e, the concentrations of T and C were then adjusted to equate the model Z_{eff}

with that of the discharge being simulated with the profile of $Z_{\rm eff}$ initially assumed to be flat. The rf power density profile was assumed to have a Gaussian form:

$$\rho_{rf}(r) = \rho_{rf}(r_0)\ exp[-(r-r_0)^2\ /\ r_d^2\ ], \tag{11}$$

where r_0 and r_d represent, respectively, the distance between the cyclotron resonance and the magnetic axis and the *e*–folding rf deposition width.

To calculate the fusion yield we used a gaussian radial power deposition profile and the explicit solution of the deuterium distribution function (STIX, 1975)

$$f(v) = f(0)\ exp - \int_0^v dv \frac{-2\alpha v^2\ +\ (\beta v^2)'}{\beta v^2\ +\ 2Kv^2}, \tag{12}$$

where α and β are the Coulomb diffusion coefficients, $K = \rho_{rf}/3n_D m_D$, and m_D is the deuteron mass. Inclusion of finite ion Larmor radius effects and, in particular, the E_ component of the rf electric field in the Fokker–Planck calculations results in a more energetic tail which tends to reduce the fusion yield compared with the Stix model. For high D minority concentration ($n_{\rm D}/n_e$ <30%), $|\,E_-|\,/|\,E_+|\ \approx\ 12$, and the reduction is typically 20%.

4 EXPERIMENTAL BASIS

We based our projections of (D)T performance on model plasmas having the same temperature and density profiles as have already been obtained experimentally on JET. Measured profiles for three types of ICRH heated discharge (JACQUINOT *et al.* 1988) were studied and used as the basis for predictions. These were: type I) 3MA peaked profile (pellet) cases (BHATNAGAR *et al.*, 1989; HAMMETT *et al.*, 1989), type II) 5MA current–rise heating cases (BURES *et al.*, 1989) and type III) 3MA 'monster' sawtooth (CAMPBELL *et al.*, 1988) cases. In the pellet fuelled discharges (Figs.6 and 7) the plasma density profiles were derived from inversion of multi–channel far–infrared (FIR) laser interferometer data and were peaked with $y(a)\ /\ y(0)\ \cong\ 0.2$ and $\gamma\ \cong\ 4$. For the electron temperature profiles (measured from electron cyclotron emission), we found $y(a)\ /\ y(0)$ =0.1 and γ=2. Fig.6 shows the temporal evolution of the plasma parameters in a typical peaked profile discharge. The FIR radial density profiles for this discharge are shown in Fig.7 In the current–rise

(CR) heating case (BURES *et al.*, 1989), application of ICRH power delayed the onset of of sawtoothing activity and allowed access of a regime with higher central electron pressure than could be obtained with applying the rf power during the current flat top (FT) phase (Fig.8). Compared with FT heating cases, the CR discharges also show a 10%–20% enhancement in global energy containment time.

The Stix model was applied (Fig.9) initially to type I discharge data assuming, for simplicity, $T_i = T_e$ and $Z_{eff}=1$. In this example, we show the effect of varying the density whilst maintaining a constant rf power and central electron pressure. We have therefore assumed the central electron energy confinement to be approximately independent of density.

4.1 *Projection to High ICRH Power*

To calculate the *DT* fusion power for applied rf heating powers higher than in the example above, it is necessary to consider the effect of the extra power on the background plasma conditions as well as the deuterium tail parameters. To do this (Fig.10), we have used measured empirical temperature scaling laws based on existing JET results. Each of the datasets for discharge types I–III could be described by the offset–linear relation:

$$T_{j0}(\mathrm{keV}) = \alpha_j + \beta_j [P_t(\mathrm{MW})/n_{e0}(10^{19}\mathrm{m}^{-3})] \qquad (13)$$

where j = electrons or ions and P_t ($\equiv P_{rf} + P_{oh}$) the total radio frequency plus ohmic input power. In making these extrapolations, we have assumed no degradation in heating efficiency (*i.e* the coefficients β_j are independent of power). The coefficients are, for type I: α_e=0.8, β_e=4.1, α_i=1.1, β_i=3.6; type II: α_e=0.8, β_e=4.1, α_i=1.1, β_i=2.6; and type III: α_e=0.7, β_e=2.7, α_i=2.3, β_i=1.2. Results for the higher power projections are given in Fig.11 showing that optimal Q values can now be obtained with higher central electron densities ($n_{e0} \approx 1 \times 10^{20}\mathrm{m}^{-3}$).

4.2 *Sensitivity Analysis and Impurity Dilution Effects*

Next we illustrate the sensitivity of the ICRH–driven fusion yield with respect to variations in resonance location (r_{0a}) for reference discharge A (Table I) assuming a

fixed rf deposition gaussian width r_d =0.2m. Variations in the fusion yield about condition A with respect to r_{oa} and Z_{eff} are shown in Fig.12. A maximum in the fusion yield occurs at $r_{oa} \approx$ 0.3m where the deuterium tail temperature is close to the maximum in the DT fusion cross–section ($T_t \cong$ 140 keV). If the ICRH power is deposited too centrally, the minority ions are driven to energies beyond the maximum in the DT cross–section and there is a reduction in fusion reactivity. Conversely, if the ICRH power is deposited too far off–axis, the tail energy falls below the maximum in the fusion cross–section and the tail is generated in a low temperature region of the plasma where the slowing–down time is small. In Fig.12, we have neglected any variations in the heating efficiency with r_{oa}. Fig.13 gives the calculated radial variations of various quantities associated with the minority tail showing both tail energy and temperature as well as DT reactivity to be peaked $\cong$ 0.3m off–axis.

In the scan of variations in Z_{eff}, we varied the assumed density of carbon impurities with a fixed value of n_D/n_T = 0.23 in the reference discharge A. Experimentally, we find that in the peaked profile (case I), the volume averaged Z_{eff} falls to $\approx$ 1 immediately following pellet injection; but $\cong$ 1 sec later, when the central electron pressure attains its peak value, Z_{eff} has risen to approximately 3. Additional spectroscopic observations show that impurities accumulate on the axis after pellet injection. For the current–rise heating case II, $Z_{eff} \approx 2$, and, in the 'monster' sawtooth case (type III), Z_{eff} values range between 4.0–2.5. We define a multiplicative fusion yield degradation factor, $\delta = [(n_T/n_e)/\ (n_T/n_e)_1]$, where $(n_T/n_e)_1$ is the triton dilution factor obtained in a Z_{eff} = 1 plasma. Fig.12 shows that the fusion power has degradation factors, δ, equal to I) 50%, II) 75% and III) 20%–66% respectively for the three types of discharge (the lower limit on δ corresponds to the upper limit of Z_{eff}). In case II), analysis of the central neutron emissivity (from the neutron profile monitor) and T_{i_0} (from neutron spectroscopy and doppler broadening of Ni impurity lines) gave a central concentration ratio n_D/n_e=90% ± 10%. If the dilution is identical when P_D=20MW (corresponding to P_{rf} = 25MW), the optimum fusion powers (for n_D/n_e=30%) are: I) $P_{fus} \approx$13MW ($Q_{rf} \approx$ 50%), II) $P_{fus} \approx$17MW ($Q_{rf} \approx$67%) and III) $P_{fus} \approx$(4–12)MW ($Q_{rf} \approx$14%–46%).

Adopting the observed experimental scaling: $Z_{eff}\ \alpha\ 1/n_e$, and extrapolating it to the optimum density ($n_{e_0} \approx\ 1\times10^{20}$ m^{-3}) shown in Fig.11, we find degradation factors: I) δ = 81%, II) δ = 96% and III) δ = 67%–92% for the three discharge types respectively. We note that both the peaked–profile (pellet) and the current–rise heating cases were not in steady–state conditions. More detailed analyses of these

discharge types can be found in BHATNAGAR *et al* (1989), HAMMETT *et al.* (1989) and BURES *et al.* (1989).

5. CONCLUSION

Based on the observed behaviour of ICRH–heated JET discharges, we have performed a theoretical study to examine the possibility of producing significant levels of ICRF–driven DT fusion reactivity in projected JET plasmas in which the deuterium has been replaced by a hypothetical mixture of deuterium and tritium. Calculations of the rf damping on the deuterium minority show that even with mixture ratios as high as $n_D/n_T \cong 40\%$, the deuterium damping is $\cong 80\%$ with most of the remainder being damped on the thermal electrons via Landau damping and TTMP. The analysis of tail reactivity in model plasmas shows the possibility of reaching Q_{rf} ($\equiv P_{fus}/P_{rf}$) $\approx$ 70% provided impurity dilution can be kept to a reasonable level. Particularly encouraging is the DT projection based on the 5MA current–rise heating case (at density $n_{e_0} = 6\times 10^{19} m^{-3}$) where values of the central electron pressure of $n_{e_0}T_{e_0} = 6\times 10^{20}$ keV m^{-3} and $Z_{eff} \approx 2.0$ have been obtained simultaneously.

ACKNOWLEDGEMENT

It is a pleasure to thank our colleagues in the JET team for assistance in this work. Particular thanks go to the tokamak operating team and to the members of the diagnostic groups involved in the measurements. We also thank P. van Belle for computing the hot deuterium–tritium cross–sections used in Fig.1.

REFERENCES

ANDERSON, D. (1983) *J.Plasma Phys.*, **29(2)**, 317.

ASHER–PERES (1979) *J. Appl Phys.*, **50(9)**, 5569.

BOYD, D.A., CAMPBELL, D.J., CORDEY, J.G., CORE, W.G.F., CHRISTIANSEN, J.P., COTTRELL, G.A., ERIKSSON, L.–G., HELLSTEN, T., JACQUINOT, J., JARVIS, O.N., KISSEL, S., LOWRY, C., NIELSEN, P., SADLER, G., START, D.F.H., THOMAS, P.R., VAN BELLE, P. and WESSON, J.A. (1989) *Nucl. Fusion.* (in press).

BHATNAGAR, V.P. *et al.* (1989) *Proc. 16th Europ. Conf. on Controlled Fusion and Plasma Physics*, Venice, Italy.

BHATNAGAR, V.P. *et al* (1984) *Nuc. Fusion* **24**, 955.

BURES, M. et al. (1989) *Proc. 16th Europ. Conf. on Controlled Fusion and Plasma Physics*, Venice, Italy.

CAMPBELL, D.J., START, D.F.H., WESSON, J.A., BARTLETT, D.V., BHATNAGAR, V.P., BURES, M., CORDEY, J.G., COTTRELL, G.A., DUPEREX, P.A., EDWARDS, A.W., CHALLIS, C.D., GORMEZANO, C., GOWERS, C.W., GRANETZ, R.S., HAMNEN, J.H., HELLSTEN, T., JACQUINOT, J., LAZZARO, E., LOMAS, P.J., LOPES CARDOZO, N., MANTICA, P., SNIPES, J.A., STORK, D., STOTT, P.E., THOMAS, P.R., THOMPSON, E., THOMSEN, K., TONETTI, G., (1989) *Phys. Rev. Lett.* **60(21)**, 2148–2151.

COTTRELL, G.A., SADLER, G., van BELLE, P., CAMPBELL, D.J., CORDEY, J.G., HELLSTEN, T., JACQUINOT, J., KISSELL, S., START, D.F.H., THOMAS, P.R., WESSON, J. (1988) *Proc. 15th Europ. Conf. on Controlled Fusion and Plasma Heating*, Dubrovnik, Yugoslavia. **12B(II)**, 721–724.

ERIKSSON, L.–G., HELLSTEN, T., BOYD, D.A., CAMPBELL, D.J., CORDEY, J.G., CORE, W.G.F., CHRISTIANSEN, J.P., COTTRELL, G.A., JACQUINOT, J., JARVIS, O.N., KISSEL, S., LOWRY, C., NIELSEN, P., SADLER, G., START, D.F.H., THOMAS, P.R., VAN BELLE, P. and WESSON, J.A. (1989) *Nucl. Fusion Lett.* **29(1)**, 87.

HAMMETT, G. *et al.* (1989) *Proc. 16th Europ. Conf. on Controlled Fusion and Plasma Physics*, Venice, Italy.

JACQUINOT, J. (1978) *Proc. of Joint Grenoble–Varenna Int. Symp. on Cont. Fusion And Plasma Heating, Grenoble, France*, **I**, 127.

JACQUINOT, J. (1988), *et al.* Bull.Amer.Phys.Soc. **33**, 2031.

JET TEAM (1988) *Plas.Phys. and Contr.Fus.* **30**, 1467.

SADLER, G. (1989) to be published.

STIX, T.H. (1975) *Nuc. Fusion*, **15**, 737.

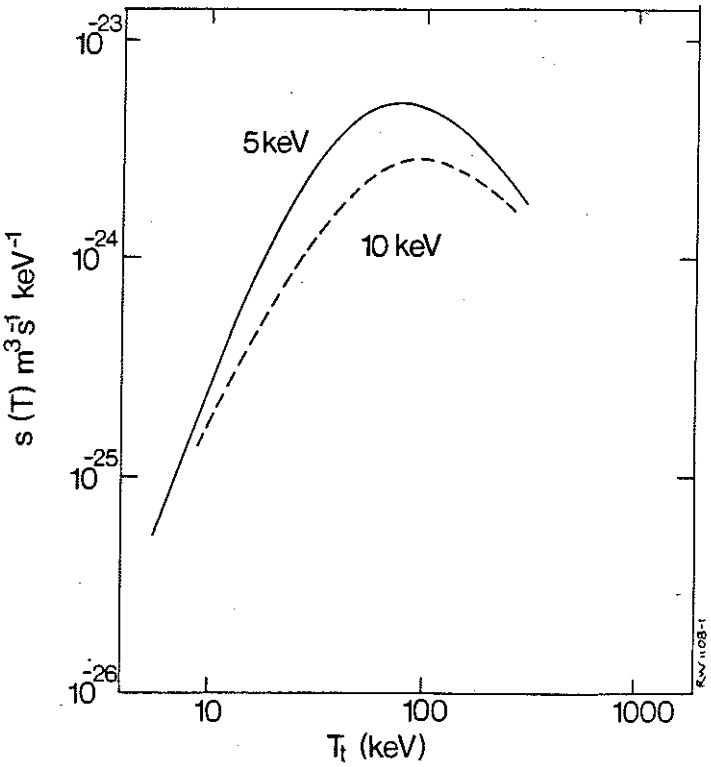

Figure 1.– Variation of the cross–section and energy–dependent (function $s(T_t)$ of Eq.(8)) with tail temperature T_t for two values of the (common) ion and electron backround temperature, $T_i = T_e = 5$ keV and 10 keV. The plasma was assumed to have $Z_{\text{eff}} = 2$ (similar to the experimental discharge type II) but with D,T and carbon impurity species.

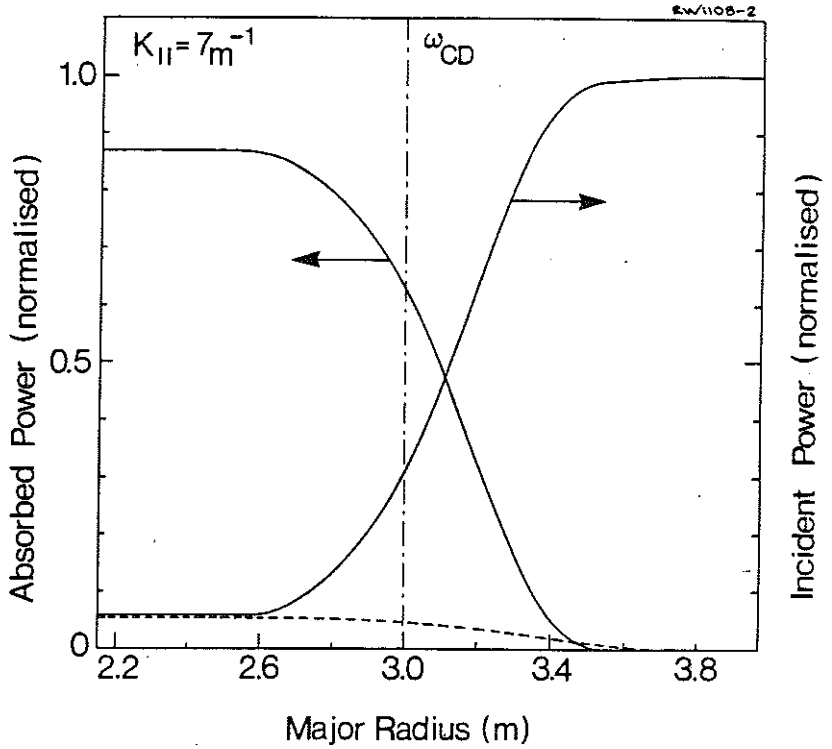

Figure 2.– Rf power fractions damped on deuterium minority (solid curve, arrow left), and electrons (dashed curve) as a function of radius for a projected $(D)T$ minority heating (reference case A, $k_{||} = 7\text{m}^{-1}$) in JET using the FREMIR wave damping code.

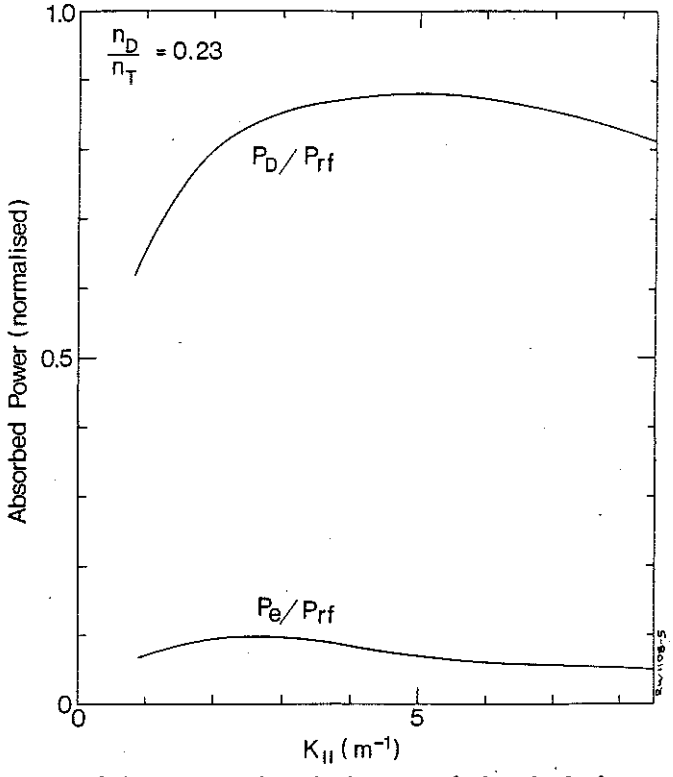

Figure 3.– FREMIR rf damping code calculations of absorbed rf power on deuterium and thermal electrons with variations in $k_{||}$ for a fixed value of the ion mixture ratio $\eta = n_D/n_T = 0.23$ and the conditions of reference discharge A.

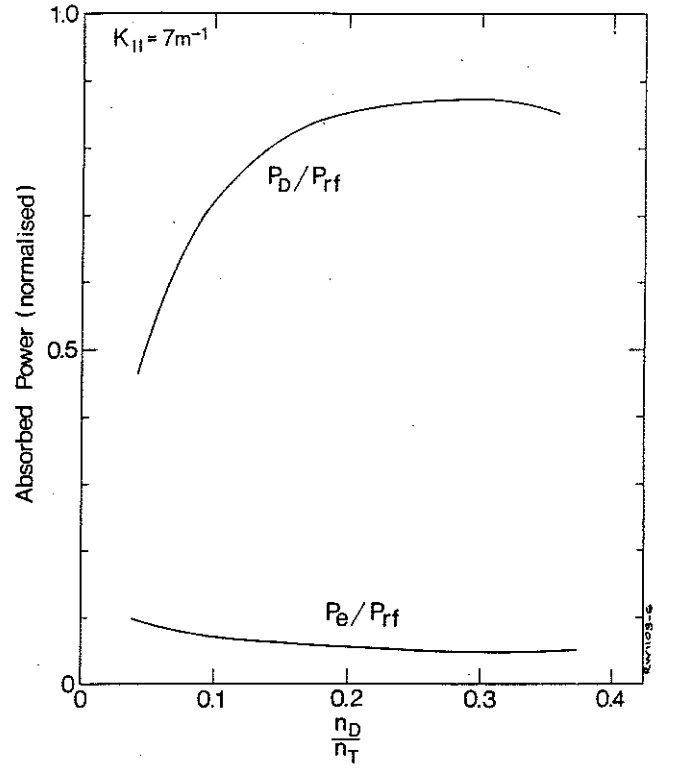

Figure 4.– FREMIR rf damping code calculations of absorbed rf power on deuterium and thermal electrons with variations in the ion mixture ratio $\eta = n_D/n_T$ for a fixed value of $k_{||} = 7m^{-1}$ and the conditions of reference discharge A.

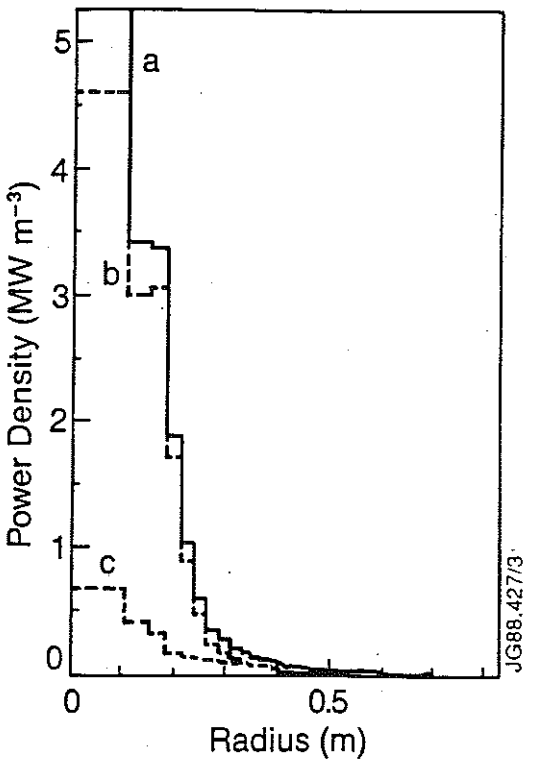

Figure 5.– Calculated ICRH deposition profiles of: a) total, b) deuterium and c) electron power densities for the case of central heating in simulated (D)T plasma based on experimental conditions of peaked–profile (pellet) discharge (Type I) but with assumed values $n_D/n_T = 0.23$ and P_D=20MW.

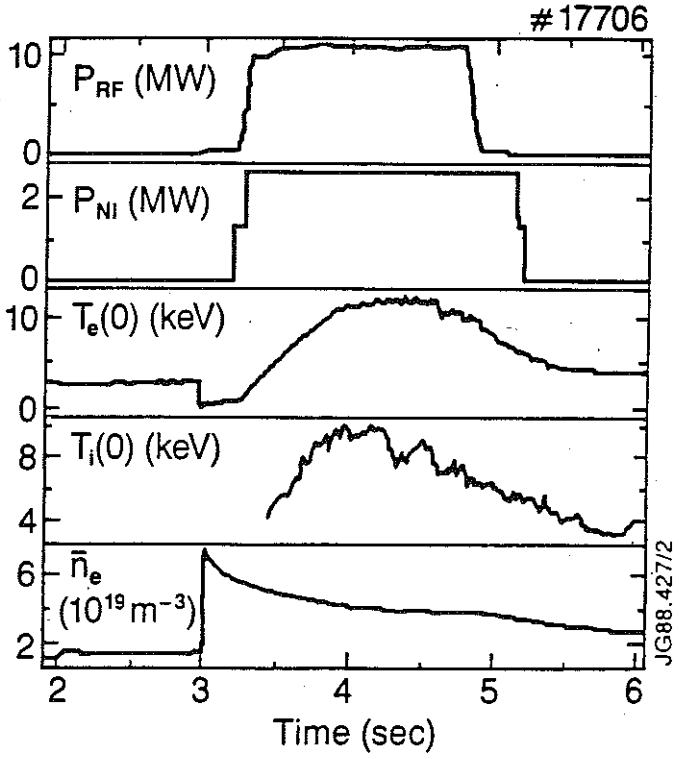

Figure 6.– Temporal evolution of plasma parameters in a peaked profile discharge (type I). A 2.7mm diameter deuterium pellet was injected at time 2 seconds followed by a 4mm diameter pellet at time 3 seconds.

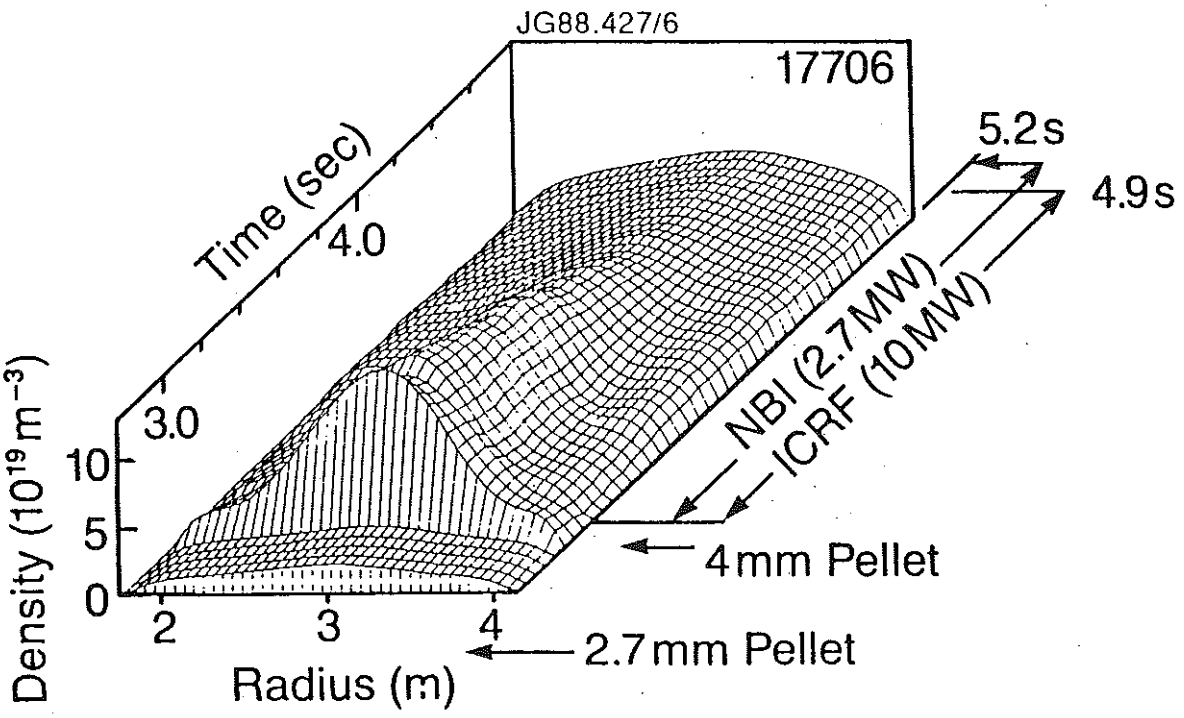

Figure 7.– Multi–chord far–infrared (FIR) laser interferometer profiles of electron density in the peaked profile discharge of Fig.6

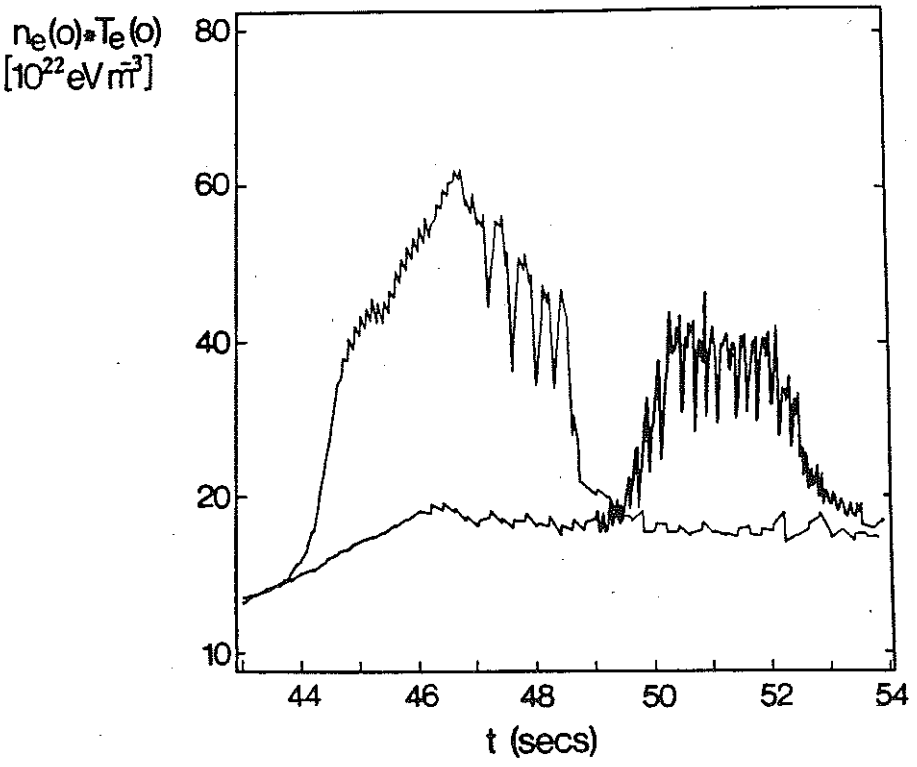

Figure 8.– Evolution of central electron pressure comparing rf heating during the current rise (Type II discharge, CR heating, narrow line) with that during the flat top (FT heating, bold line). The two discharges were otherwise similar with P_{rf} = 11MW and I_p = 5MA.

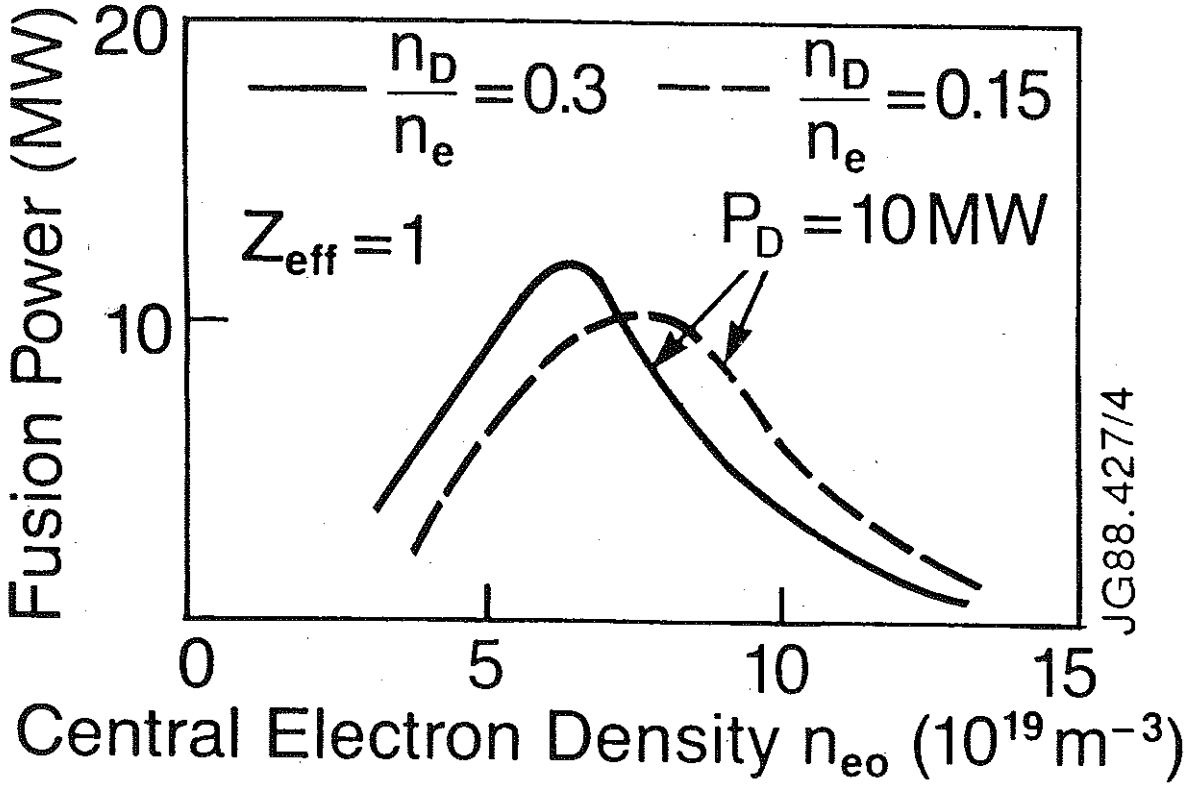

Figure 9.– Stix code results for ICRH driven DT fusion power with fixed central electron pressure $n_{e_0} T_{e_0} = 6 \times 10^{20}$ keV m^{-3} and damped rf power P_D = 10MW (P_{rf} = 12MW). Off–axis (r_{0a}= 0.3m) rf heating was modelled with gaussian deposition width r_d =0.2m.

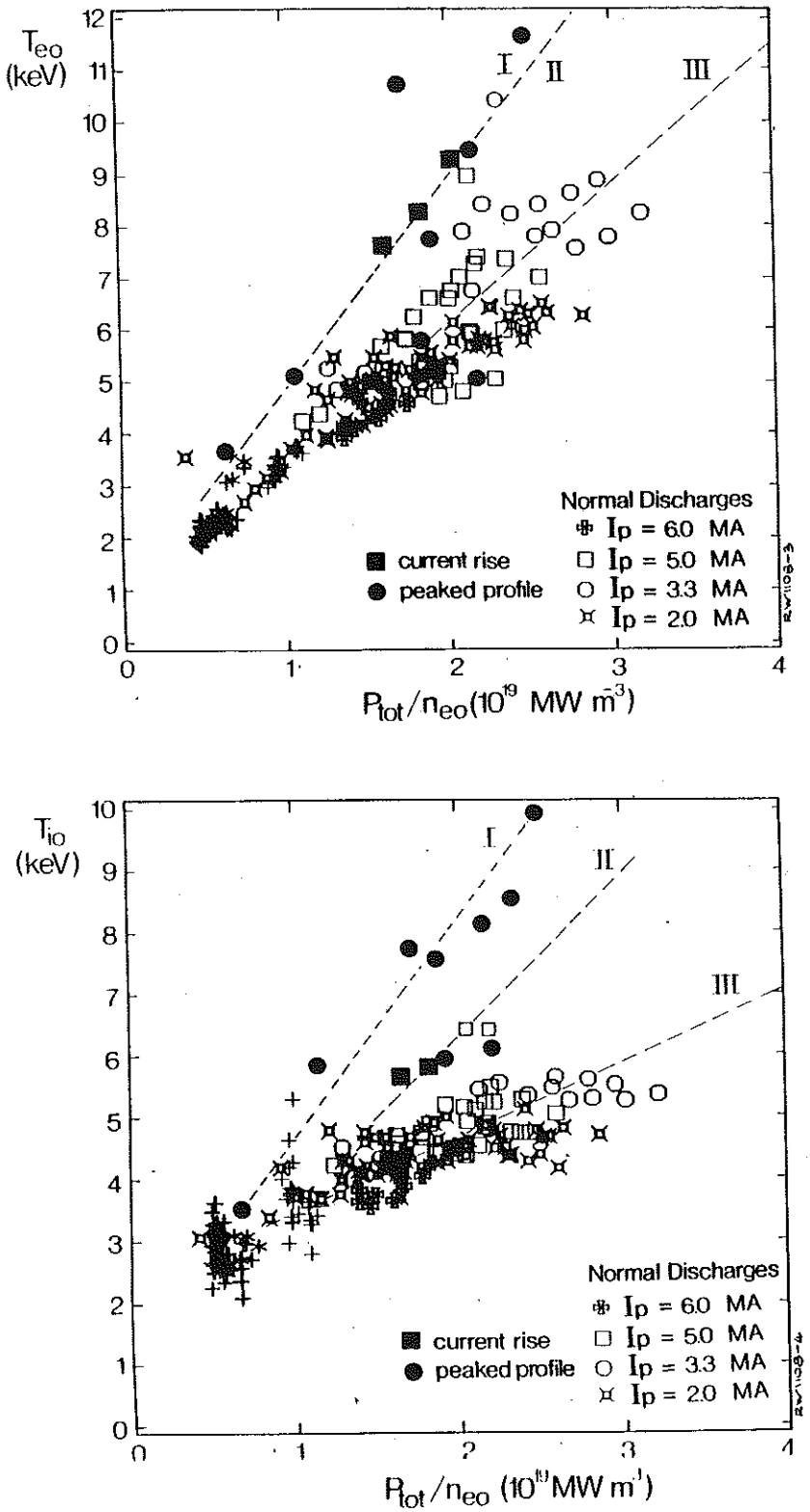

Figure 10.– Variation of central (a) electron and (b) ion temperatures with P_t/n_{e_0} for each of the three types of ICRH discharge studied. The fitted lines were used to obtain the coefficients in the offset–linear temperature scaling laws.

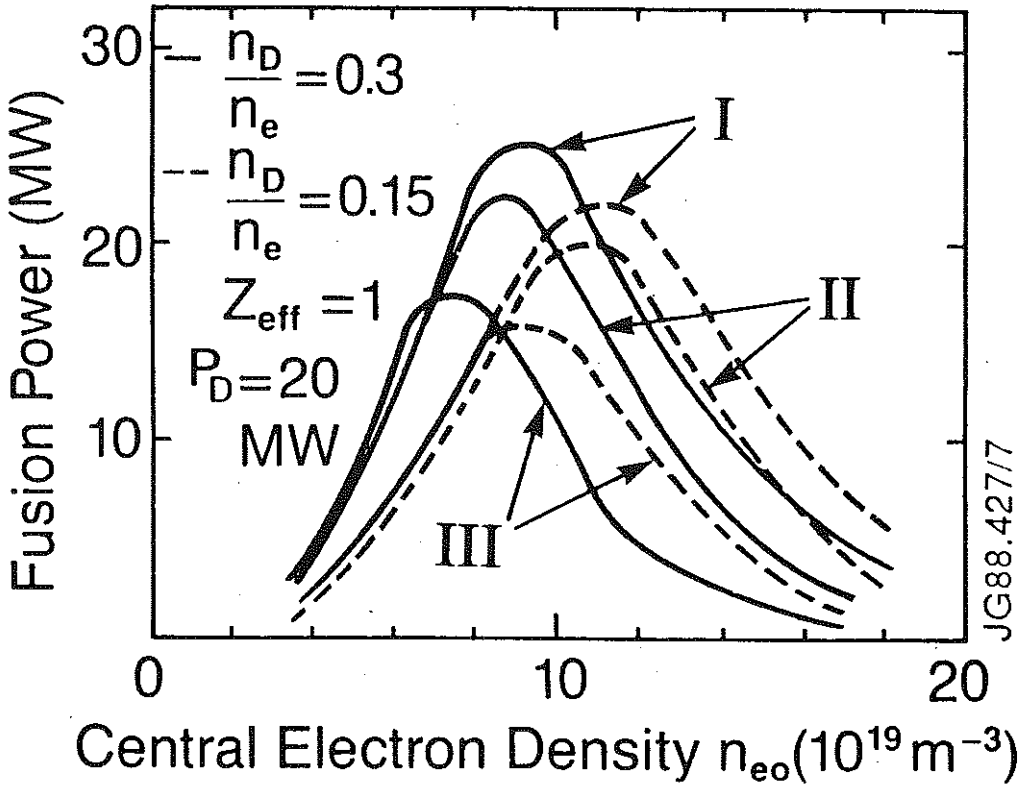

Figure 11.– Stix code results for three projected cases (with P_{rf} = 25MW, P_D= 20MW): I) peaked profiles (pellet injection), II) current–rise heating and III) 'monster' sawtooth cases. Off–axis (r_{oa}=0.3m) rf heating was modelled with gaussian deposition width r_d = 0.2m.

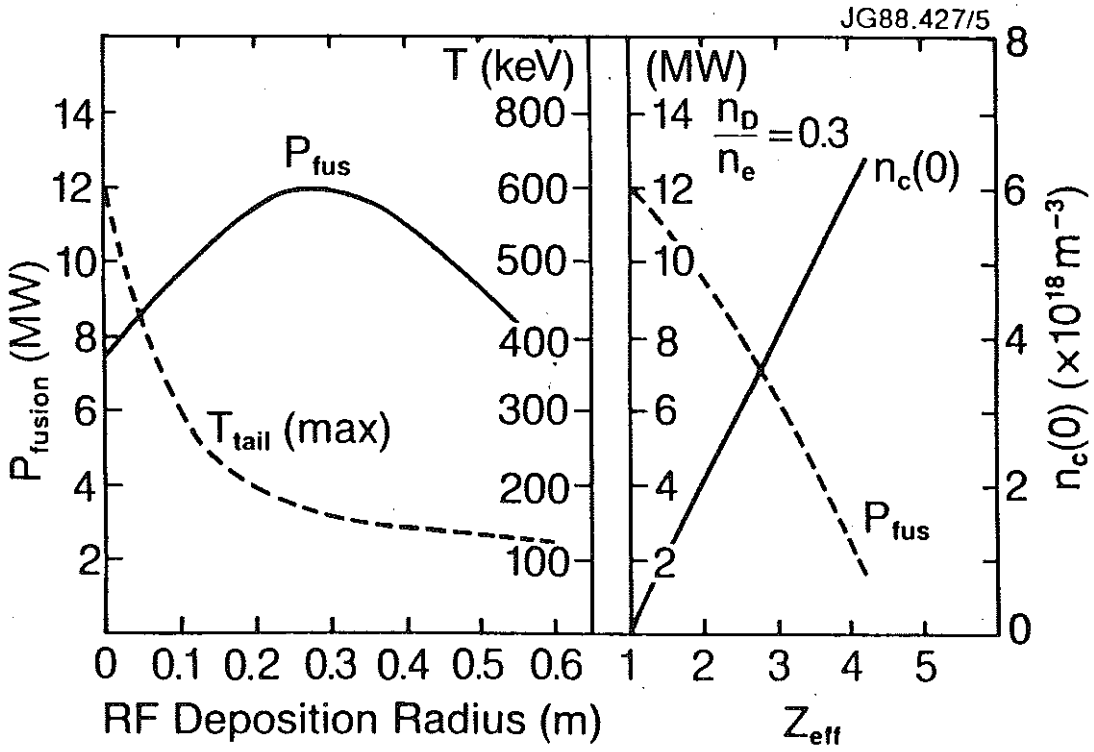

Figure 12.– Sensitivity analysis (case A) of the variation of a) DT fusion power and minority tail temperature with rf power off–axis displacement and, b) DT fusion power and carbon impurity density with Z_{eff}.

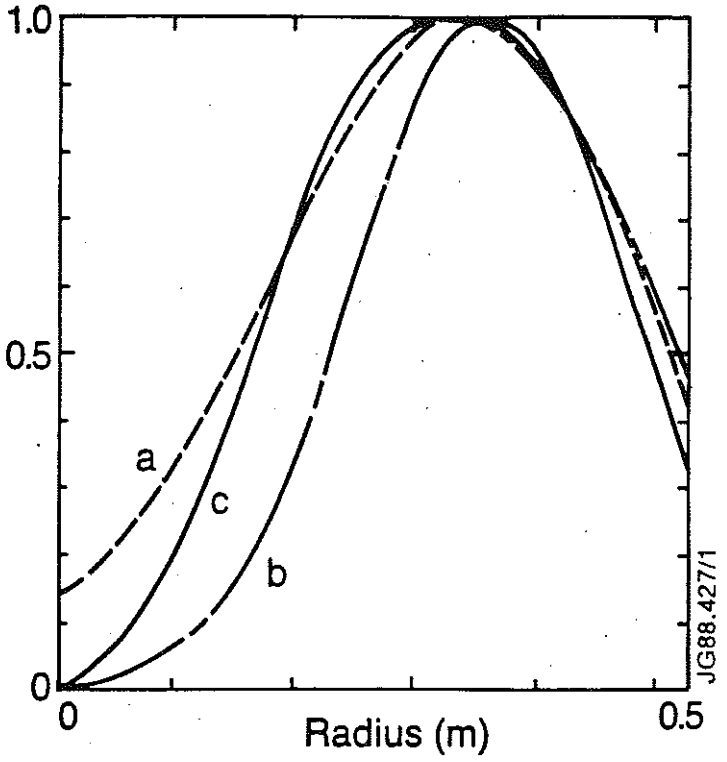

Figure 13.– Calculated radial variations of (a) tail temperature (maximum value = 140 keV), (b) kinetic energy and (c) fusion reactivity for the reference discharge A.

APPENDIX 1.

THE JET TEAM

JET Joint Undertaking, Abingdon, Oxon, OX14 3EA, U.K.

J.M.Adams[1], F.Alladio[4], H.Altmann, R.J.Anderson, G.Appruzzese, W.Bailey, B.Balet, D.V.Bartlett, L.R.Baylor[24], K.Behringer, A.C.Bell, P.Bertoldi, E.Bertolini, V.Bhatnagar, R.J.Bickerton, A.Boileau[3], T.Bonicelli, S.J.Booth, G.Bosia, M.Botman, D.Boyd[31], H.Brelen, H.Brinkschulte, M.Brusati, T.Budd, M.Bures, T.Businaro[4], H.Buttgereit, D.Cacaut, C.Caldwell-Nichols, D.J.Campbell, P.Card, J.Carwardine, G.Celentano, P.Chabert[27], C.D.Challis, A.Cheetham, J.Christiansen, C.Christodoulopoulos, P.Chuilon, R.Claesen, S.Clement[30], J.P.Coad, P.Colestock[6], S.Conroy[13], M.Cooke, S.Cooper, J.G.Cordey, W.Core, S.Corti, A.E.Costley, G.Cottrell, M.Cox[7], P.Cripwell[13], F.Crisanti[4], D.Cross, H.de Blank[16], J.de Haas[16], L.de Kock, E.Deksnis, G.B.Denne, G.Deschamps, G.Devillars, K.J.Dietz, J.Dobbing, S.E.Dorling, P.G.Doyle, D.F.Düchs, H.Duquenoy, A.Edwards, J.Ehrenberg[14], T.Elevant[12], W.Engelhardt, S.K.Erents[7], L.G.Eriksonn[5], M.Evrard[2], H.Falter, D.Flory, M.Forrest[7], C.Froger, K.Fullard, M.Gadeberg[11], A.Galetsas, R.Galvao[8], A.Gibson, R.D.Gill, A.Gondhalekar, C.Gordon, G.Gorini, C.Gormezano, N.A.Gottardi, C.Gowers, B.J.Green, F.S.Griph, M.Gryzinski[26], R.Haange, G.Hammett[6], W.Han[9], C.J.Hancock, P.J.Harbour, N.C.Hawkes[7], P.Haynes[7], T.Hellsten, J.L.Hemmerich, R.Hemsworth, R.F.Herzog, K.Hirsch[14], J.Hoekzema, W.A.Houlberg[24], J.How, M.Huart, A.Hubbard, T.P.Hughes[32], M.Hugon, M.Huguet, J.Jacquinot, O.N.Jarvis, T.C.Jernigan[24], E.Joffrin, E.M.Jones, L.P.D.F.Jones, T.T.C.Jones, J.Källne, A.Kaye, B.E.Keen, M.Keilhacker, G.J.Kelly, A.Khare[15], S.Knowlton, A.Konstantellos, M.Kovanen[21], P.Kupschus, P.Lallia, J.R.Last, L.Lauro-Taroni, M.Laux[33], K.Lawson[7], E.Lazzaro, M.Lennholm, X.Litaudon, P.Lomas, M.Lorentz-Gottardi[2], C.Lowry, G.Magyar, D.Maisonnier, M.Malacarne, V.Marchese, P.Massmann, L.McCarthy[28], G.McCracken[7], P.Mendonca, P.Meriguet, P.Micozzi[4], S.F.Mills, P.Millward, S.L.Milora[24], A.Moissonnier, P.L.Mondino, D.Moreau[17], P.Morgan, H.Morsi[14], G.Murphy, M.F.Nave, M.Newman, L.Nickesson, P.Nielsen, P.Noll, W.Obert, D.O'Brien, J.O'Rourke, M.G.Pacco-Düchs, M.Pain, S.Papastergiou, D.Pasini[20], M.Paume[27], N.Peacock[7], D.Pearson[13], F.Pegoraro, M.Pick, S.Pitcher[7], J.Plancoulaine, J-P.Poffé, F.Porcelli, R.Prentice, T.Raimondi, J.Ramette[17], J.M.Rax[27], C.Raymond, P-H.Rebut, J.Removille, F.Rimini, D.Robinson[7], A.Rolfe, R.T.Ross, L.Rossi, G.Rupprecht[14], R.Rushton, P.Rutter, H.C.Sack, G.Sadler, N.Salmon[13], H.Salzmann[14], A.Santagiustina, D.Schissel[25], P.H.Schild, M.Schmid, G.Schmidt[6], R.L.Shaw, A.Sibley, R.Simonini, J.Sips[16], P.Smeulders, J.Snipes, S.Sommers, L.Sonnerup, K.Sonnenberg, M.Stamp, P.Stangeby[19], D.Start, C.A.Steed, D.Stork, P.E.Stott, T.E.Stringer, D.Stubberfield, T.Sugie[18], D.Summers, H.Summers[20], J.Taboda-Duarte[22], J.Tagle[30], H.Tamnen, A.Tanga, A.Taroni, C.Tebaldi[23], A.Tesini, P.R.Thomas, E.Thompson, K.Thomsen[11], P.Trevalion, M.Tschudin, B.Tubbing, K.Uchino[29], E.Usselmann, H.van der Beken, M.von Hellermann, T.Wade, C.Walker, B.A.Wallander, M.Walravens, K.Walter, D.Ward, M.L.Watkins, J.Wesson, D.H.Wheeler, J.Wilks, U.Willen[12], D.Wilson, T.Winkel, C.Woodward, M.Wykes, I.D.Young, L.Zannelli, M.Zarnstorff[6], D.Zasche[14], J.W.Zwart.

PERMANENT ADDRESS

1. UKAEA, Harwell, Oxon. UK.
2. EUR-EB Association, LPP-ERM/KMS, B-1040 Brussels, Belgium.
3. Institute National des Récherches Scientifique, Quebec, Canada.
4. ENEA-CENTRO Di Frascati, I-00044 Frascati, Roma, Italy.
5. Chalmers University of Technology, Göteborg, Sweden.
6. Princeton Plasma Physics Laboratory, New Jersey, USA.
7. UKAEA Culham Laboratory, Abingdon, Oxon. UK.
8. Plasma Physics Laboratory, Space Research Institute, Sao José dos Campos, Brazil.
9. Institute of Mathematics, University of Oxford, UK.
10. CRPP/EPFL, 21 Avenue des Bains, CH-1007 Lausanne, Switzerland.
11. Risø National Laboratory, DK-4000 Roskilde, Denmark.
12. Swedish Energy Research Commission, S-10072 Stockholm, Sweden.
13. Imperial College of Science and Technology, University of London, UK.
14. Max Planck Institut für Plasmaphysik, D-8046 Garching bei München, FRG.
15. Institute for Plasma Research, Gandhinagar Bhat Gujat, India.
16. FOM Instituut voor Plasmafysica, 3430 Be Nieuwegein, The Netherlands.
17. Commissiariat à L'Energie Atomique, F-92260 Fontenay-aux-Roses, France.
18. JAERI, Tokai Research Establishment, Tokai-Mura, Naka-Gun, Japan.
19. Institute for Aerospace Studies, University of Toronto, Downsview, Ontario, Canada.
20. University of Strathclyde, Glasgow, G4 ONG, U.K.
21. Nuclear Engineering Laboratory, Lapeenranta University, Finland.
22. JNICT, Lisboa, Portugal.
23. Department of Mathematics, Univeristy of Bologna, Italy.
24. Oak Ridge National Laboratory, Oak Ridge, Tenn., USA.
25. G.A. Technologies, San Diego, California, USA.
26. Institute for Nuclear Studies, Swierk, Poland.
27. Commissiariat à l'Energie Atomique, Cadarache, France.
28. School of Physical Sciences, Flinders University of South Australia, South Australia SO42.
29. Kyushi University, Kasagu Fukuoka, Japan.
30. Centro de Investigaciones Energeticas Medioambientales y Techalogicas, Spain.
31. University of Maryland, College Park, Maryland, USA.
32. University of Essex, Colchester, UK.
33. Akademie de Wissenschaften, Berlin, DDR.

CR 88.49.1A